CONDENSED MATTER PHYSICS

Controllable freezing of the nuclear spin bath in a single-atom spin qubit

Mateusz T. Mądzik[1], Thaddeus D. Ladd[2,3], Fay E. Hudson[1], Kohei M. Itoh[4], Alexander M. Jakob[5], Brett C. Johnson[5], Jeffrey C. McCallum[5], David N. Jamieson[5], Andrew S. Dzurak[1], Arne Laucht[1], Andrea Morello[1]*

The quantum coherence and gate fidelity of electron spin qubits in semiconductors are often limited by nuclear spin fluctuations. Enrichment of spin-zero isotopes in silicon markedly improves the dephasing time T_2^*, which, unexpectedly, can extend two orders of magnitude beyond theoretical expectations. Using a single-atom ^{31}P qubit in enriched ^{28}Si, we show that the abnormally long T_2^* is due to the freezing of the dynamics of the residual ^{29}Si nuclei, caused by the electron-nuclear hyperfine interaction. Inserting a waiting period when the electron is controllably removed unfreezes the nuclear dynamics and restores the ergodic T_2^* value. Our conclusions are supported by a nearly parameter-free modeling of the ^{29}Si nuclear spin dynamics, which reveals the degree of backaction provided by the electron spin. This study clarifies the limits of ergodic assumptions in nuclear bath dynamics and provides previously unidentified strategies for maximizing coherence and gate fidelity of spin qubits in semiconductors.

INTRODUCTION

Electron spin qubits in semiconductors are prominent candidates for building blocks of scalable quantum computers, thanks to a combination of small physical size, long quantum coherence times, and potential manufacturability using industry-standard processes (*1*, *2*). Demonstrating a universal set of quantum gates with fidelities beyond the fault-tolerance threshold remains the main focus of current research in the field.

Microscopically, one of the main sources of decoherence and gate errors is the coupling between the electron spin qubit and the mesoscopic bath of nuclear spins present in the host semiconductor material. The fluctuating polarization of the nuclear spin bath produces an effective magnetic field noise, which results in a random component of the instantaneous value of the qubit resonance frequency. This randomness affects the qubit coherence time, since the precise rate of phase accumulation is no longer accurately known, and the quantum gate fidelities, since the frequency of the classical control fields may be off-resonance with the instantaneous precession frequency of the spin qubit.

Silicon, the material underpinning all of the modern microelectronic industry, also has the key property of having a large natural abundance of the spin-zero nuclear isotope ^{28}Si, whereas only 4.7% ^{29}Si nuclei carry a spin $I = 1/2$. Isotopic enrichment methods compatible with wafer-scale fabrication have provided ^{29}Si concentrations of orders 500 to 800 parts per million (ppm) (*3*, *4*). As was known for decades (*5*), and more recently studied in detail in ensemble experiments on ^{31}P donors in silicon (*6*, *7*), the electron spin coherence (as measured by a Hahn echo) in these enriched ^{28}Si substrates is substantially improved from the values found in natural silicon. There is excellent agreement between measurements of an electron spin Hahn echo decay in donor ensembles and their predicted behavior based on the theoretical description of ^{29}Si nuclear spin dynamics (*8*, *9*).

A series of experiments has been carried out in recent years on single–donor ion–implanted spin qubit devices in enriched silicon with 800-ppm residual ^{29}Si. These experiments have qualitatively confirmed that the enrichment of spin-zero isotopes improves spin coherence times (*10*) and quantum gate fidelities (*11*, *12*). The Hahn echo decay time (see the "Experimental evidence of nuclear freezing by hyperfine interactions" section for a description of the Hahn echo method), $T_2^{\mathrm{Hahn}} \approx 200$ μs in natural silicon (*13*), was shown to increase by a factor of ~5 in enriched ^{28}Si (*10*). However, the "pure dephasing" time T_2^* obtained in a Ramsey experiment went from $T_2^* \approx 55$ ns in natural silicon to $T_2^* \approx 270$ μs in 800-ppm material, an improvement of over three orders of magnitude. Notably, this surpasses by nearly two orders of magnitude what would be predicted, assuming an ergodic behavior of the spin polarization of the residual ^{29}Si nuclei.

The expected value of T_2^* for electron spin qubits coupled to a nuclear spin bath can be obtained by the following simple consideration (*14*, *15*). Suppose that, over a sequence of experiments on an electron spin qubit, the system samples with equal probability every possible configuration of the nuclear spins coupled to the qubit. The total electron-nuclear interaction is described by the Hamiltonian

$$H_{\mathrm{HF}} = \sum_j A_j I_j^z S^z \qquad (1)$$

where A_j is a hyperfine coupling coefficient (dominated by the Fermi contact term) between the electron and the jth nucleus, I_j^z is the z component of the spin operator for nucleus j, and S^z is the z component of the spin operator for the electron. In a semiclassical picture, the hyperfine Hamiltonian above can be thought of resulting in a longitudinal magnetic field B_{HF} coupling to the electron (Overhauser field). This Hamiltonian assumes a large applied magnetic field B_0 in the z direction, which allows neglecting the terms that do not conserve Zeeman energy (our experiments use $B_0 = 1.4$ T, corresponding to an electron Larmor frequency of ~40 GHz, far exceeding the

[1]Centre for Quantum Computation and Communication Technology, School of Electrical Engineering and Telecommunications, UNSW Sydney, Sydney, NSW 2052, Australia. [2]School of Physics, UNSW Sydney, Sydney, NSW 2052, Australia. [3]HRL Laboratories, LLC, 3011 Malibu Canyon Rd., Malibu, CA 90265, USA. [4]School of Fundamental Science and Technology, Keio University, Kohoku-ku, Yokohama, Japan. [5]Centre for Quantum Computation and Communication Technology, School of Physics, University of Melbourne, Melbourne, VIC 3010, Australia.
*Corresponding author. Email: a.morello@unsw.edu.au

values of A_j/h, typically of order megahertz or less). If we could presume a sufficiently long averaging time to ensure that the fluctuations in the nuclear bath eventually lead the system to sample all possible nuclear spin configurations, then the variance of the Overhauser field B_{HF} would be found as the sum of the variances of equal binomial random variables for each nuclear spin, giving a total variance σ_ω in the Larmor frequency ω_e of the electron spin

$$\sigma_\omega^2 = \frac{2}{(T_{2\infty}^*)^2} = \frac{I(I+1)}{3}\sum_j A_j^2 \quad (2)$$

As a result, electron coherences would follow a Gaussian decay of the form $\exp[-(\sigma_\omega t)^2/2]$. These presumptions describe the ergodic limit for T_2^*, here notated as $T_{2\infty}^*$, which takes the value $T_{2\infty}^* = \sqrt{2}/\sigma_\omega$ according to Eq. 2. The underlying noise process that drives the system to its ergodic limit is often further captured by describing it via spin diffusion resulting from the nuclear dipole-dipole interaction, leading to a local power spectral density (PSD) proportional to $1/\omega^2$ (*16*–*18*).

In the case of a ^{31}P donor in silicon, the hyperfine constants for nearby ^{29}Si, A_j, are known, and tabulated in (*19*). In a radius of 3.5-nm sphere around the ^{31}P, A_j has a mean value across all sites of ≈160 kHz, an SD of ≈340 kHz, and a maximum of 6 MHz. An important difference between donors in silicon and paramagnetic impurities in crystals with a simpler band structure is the fact that A_j does not vary monotonically with the distance between each ^{29}Si nucleus and the ^{31}P donor. This is due to the sixfold degenerate conduction band minima of silicon, causing valley interference in the wave function of bound electron states. Nonetheless, we may use these tabulated values and evaluate a large ensemble of random ^{29}Si placements at 800-ppm concentration to find that σ_ω^2 is log-normal distributed as $10^{0.4\pm0.7}$ $(\mathrm{rad/s})^2$. The probability of a random placement of nuclear spins providing $T_{2\infty}^* > 200$ μs is therefore less than 1 in 50 million. This begs the question as to why observed dephasing times are two orders of magnitude larger than a reasonable value for $T_{2\infty}^*$. The question is particularly pressing in view of the fact that, also in the case of pure dephasing times (or its inverse, the inhomogenous linewidth), theory and experiments agree very well in the case of spin ensembles (*20*). It is also pressing because the fidelity of two-qubit logic operations, or their control resources for noise compensation, depends more crucially on the pure dephasing time than on the Hahn echo time (*21*).

Understanding the microscopic reason why the single-spin experimental results consistently deviate from the ergodic model is the aim of this work. We present a simple experiment, designed to provide a clear insight into what freezes the dynamics of the ^{29}Si spin bath. The experiment shows the ability to control the dynamics of the nuclear bath and, in turn, approaching the spin dephasing values expected from an ergodic assumption. We have repeated the key parts of the experiment on three nominally identical single-donor devices (labeled devices A, B, and C in the rest of the paper) to verify that, despite the random and uncontrollable placement of the sparse ^{29}Si nuclei around each donor, our observation have general validity.

We then provide a detailed and nearly parameter-free theoretical model that puts our observation in a quantitative framework and reveals important details on the interplay between qubit measurement and nuclear bath dynamics. By using the ^{31}P donor system in 800-ppm enriched silicon, the small (of order 10 within the electron Bohr radius) number of ^{29}Si nuclei involved allows us to treat the problem in a brute-force, numerically accurate way.

Our work provides insights into decoherence processes that could not, even in principle, be obtained from experiments on spin ensembles. By definition, the local Overhauser field averaged over a large spin ensemble will exhibit statistics that reflect the distribution of all possible ^{29}Si nuclear spin configurations (unless some hyperpolarization method is applied). Therefore, only a single-spin experiment can unveil the precise statistics and time scales over which the Overhauser field actually explores the whole range allowed by the nuclear spin concentration. In addition, our theoretical model includes explicitly the backaction of the electron spin measurement on the nuclear bath. This turned out to be a key ingredient to fully describe the qubit and bath dynamics, also unavailable from ensemble magnetic resonance experiments.

RESULTS

Experimental evidence of nuclear freezing by hyperfine interactions

The design of our experiment aims at testing the "nuclear freezing" hypothesis, which postulates the existence of a "frozen core" of nuclear spins located within a "spin diffusion barrier" close to the electron spin (*22*, *23*). The dynamics of these nuclear spins is frozen by the presence of electron-nuclear hyperfine interactions that vary strongly at each lattice site, causing the nuclear spins to have markedly different energy splittings. As a consequence, energy-conserving nuclear flip-flop processes are strongly suppressed, since the nuclear dipole-dipole interaction is much weaker than the energy difference caused by the local variation of hyperfine couplings. Experimental evidence for the existence of a diffusion barrier for nuclear spins was given by Wolfe in 1973 (*24*). Key signatures of nuclear freezing effects also appear in combined optical and magnetic resonance studies of single defects (*25*), decoherence in molecular magnets (*26*), and in dynamic nuclear polarization (*27*, *28*).

Here, we aim at providing direct evidence of the impact of nuclear freezing on the dephasing of a single electron spin qubit in silicon, using a novel method where the barrier to nuclear spin diffusion can be forcibly removed.

Beside the novelty of our experimental method, we note a couple features particular to silicon. First, the standard models of "diffusion barriers" should be used with some care when studying electronic spins in silicon. This is because the hyperfine couplings have an oscillatory character as a function of the distance from the impurity. The frozen nuclear spins are not contained within a well-defined radius beyond which spin diffusion is allowed, as indicated in prior studies (*24*–*28*).

Second, in other materials such as GaAs, additional mechanisms exist for freezing the nuclear spin dynamics, caused by the nonzero quadrupole moment of the nuclei (e.g., ^{69}Ga, ^{71}Ga, and ^{75}As), which can couple to strain (*29*) and electric field gradients (*30*) to induce local shifts in individual nuclear energy splittings. Since the $I = 1/2$ ^{29}Si nuclei have zero quadrupole moment, these freezing mechanisms do not exist in silicon. Therefore, our system provides a clean and simple platform in which to study nuclear spin freezing by hyperfine and dipole-dipole effects alone.

The major distinction in the present experiment relative to other systems previously studied is the deliberate use of our ability to ionize single phosphorus donors in gated nanostructures (*31*), allowing us to "unfreeze" nuclear spins on demand (Fig. 1). Figure 2 (A and E) shows the basic schematic of the experimental protocol, in which

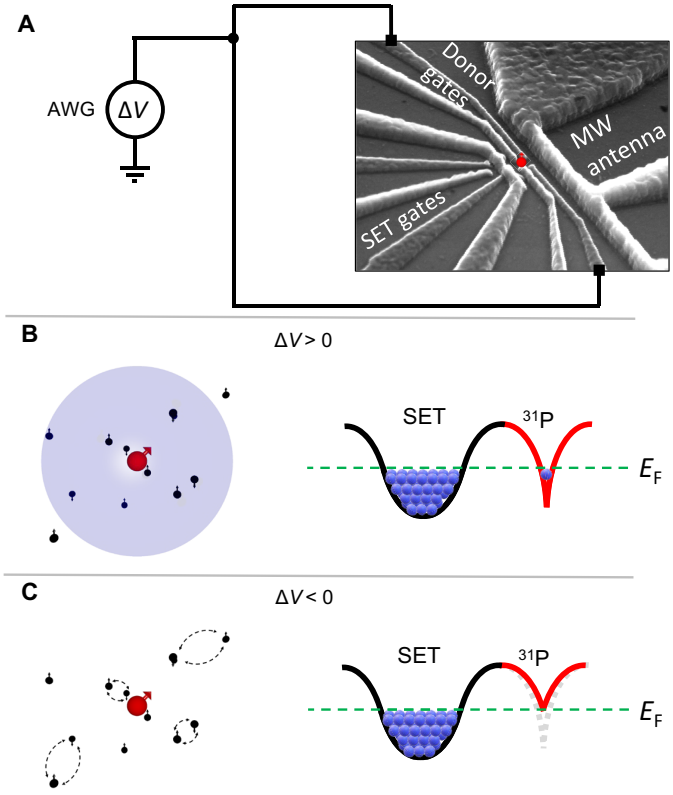

Fig. 1. Charge-state control in single-atom spin qubit devices. (**A**) Scanning electron micrograph of a device similar to those used for the experiments. ^{31}P donors are introduced by ion implantation in the vicinity of a nanofabricated single-electron transistor (SET). A broadband, on-chip microwave antenna delivers coherent spin-resonance pulses. Electrostatic gates, connected to an arbitrary waveform generator (AWG), control the donor electrochemical potential. (**B**) A positive donor gate voltage ensures that the donor is in the neutral charge state, where an electron is loosely bound to the ^{31}P nucleus and couples via contact hyperfine interaction to a sparse bath of ^{29}Si nuclei. (**C**) A negative donor gate voltage raises the donor potential above the Fermi energy E_F. The tunnel coupling between donor and SET island allows the electron to escape, leaving the donor in an ionized state. The hyperfine coupling to the ^{29}Si nuclei thus disappears.

we perform measurements of T_2^* using the Ramsey technique while maintaining the donor in different ionization states between each individual run. First, the donor system is initialized in the ground electron $|\downarrow\rangle$ state. The ^{31}P nuclear spin is set in the $|\Uparrow\rangle$ state and remains unchanged during the entire duration of the experiment. From here onward, the ^{31}P nucleus will be ignored, since it plays no role other than providing a constant hyperfine frequency shift, i.e., causing the nominal electron spin Larmor frequency to be $\omega_e = \gamma_e B_0 + A_P/2$, where $\gamma_e/2\pi \approx 28$ GHz/T is the electron gyromagnetic ratio, and $A_P/2\pi \approx 100$ MHz is the hyperfine coupling to the ^{31}P nucleus. Then, a microwave electron spin resonance (ESR) $\pi/2$ pulse at frequency ω_{MW} establishes an electron spin coherence of the form $\left(|\downarrow\rangle + e^{i\phi_0}|\uparrow\rangle\right)/\sqrt{2}$ (we can set $\varphi_0 = 0$ as the result of the first pulse). This coherence evolves freely for a time τ; if the electron Larmor frequency had been exactly ω_{MW} during the free evolution time τ, then the initial superposition state $\left(|\downarrow\rangle + |\uparrow\rangle\right)/\sqrt{2}$ would remain unchanged when observed in the rotating frame of the microwave source. Therefore, a second $\pi/2$ pulse would cause the final state of the spin to be simply $|\uparrow\rangle$, verifiable by a subsequent single-shot measurement of the electron spin (*32*).

Including now the effect of the bath nuclear spins, described in a simple picture by a time-dependent Overhauser field $B_{HF}(t)$, the instantaneous electron Larmor frequency becomes $\omega_e + \delta\omega_e(t)$, where $\delta\omega_e(t) = \gamma_e B_{HF}(t)$. After the first $\pi/2$ pulse at time t, and the free evolution time τ, the electron coherence becomes $\left(|\downarrow\rangle + e^{i\phi_0}|\uparrow\rangle\right)/\sqrt{2}$, where the accumulated phase is $\phi_\tau = \int_t^{t+\tau} dt' \delta\omega_e(t')$. This accumulated phase determines the final state after the second $\pi/2$ pulse: for example, if $\phi_\tau = \pi$, then the second pulse has the effect of flipping the electron spin back to $|\downarrow\rangle$.

We call a "single run" the following sequence of operations: initialize $|\downarrow\rangle$ – $\pi/2$ pulse, wait τ, $\pi/2$ pulse, and single-shot spin measurement. The probability $P_\uparrow^i$ of measuring $|\uparrow\rangle$ at the end of the ith run is thus $P_\uparrow^i(\tau) = \cos^2(\phi_\tau^i/2)$. We perform 100 inidividual runs at each value of τ to extract the average electron spin-up fraction $P_\uparrow(\tau)$. The Ramsey experiment is completed by repeating the above operations for 100 different values of τ. Choosing the microwave frequency with a deliberate detuning from the Larmor frequency, $\Delta\omega = \omega_e - \omega_{MW}$, causes the appearance of Ramsey fringes due to the phase accumulation $\phi_\tau = \Delta\omega \cdot \tau$, which is reflected in the oscillatory behavior of $P_\uparrow(\tau) = \cos^2(\phi_\tau/2)$. As long as $\Delta\omega$ (and therefore, B_{HF}) is constant, however, the amplitude of the Ramsey fringes does not decay with τ. This would be true even in the presence of an a priori unknown, but constant, Overhauser field. What causes Ramsey decay is the time-dependent fluctuations of $\delta\omega_{te}(t)$ between individual experimental runs. If $B_{HF}(t)$ changes from run to run, then so does $P_\uparrow^i(\tau)$ in each run. When the range of variation of B_{HF} causes $P_\uparrow^i(\tau)$ to take any possible value between 0 and 1, the averaged Ramsey fringes decay to $P_\uparrow = 0.5$. The $1/e$ decay time of the Ramsey fringes as a function of τ, extracted via fit to Gaussian decay, is used as the definition of T_2^*.

The key novelty in our protocol is the insertion of a wait time T_{wait} before each individual run. We perform two sets of identical Ramsey experiments, but in one set, the wait time T_{wait} is spent with the donor in the neutral charge state (Fig. 2A), while in the other set, the donor is kept ionized (Fig. 2E). This protocol intends to test the hypothesis that, while the donor is in the neutral state, its nuclear spin bath is "frozen" by the presence of the electron. The extra wait time is thus unlikely to cause a change in the Overhauser field between runs. In the ionized case, instead, the absence of the electron allows the bath nuclear spins to undergo energy-conserving flip-flop dynamics mediated by their mutual magnetic dipole interaction. Once the electron is reintroduced to take the next run, it is likely to find the bath in a different state from the previous run. This is expected to lead to a drastic reduction in the observed T_2^*.

In Fig. 2, we report the individual Ramsey decays obtained by repeating the protocol for three different wait times T_{wait} = 100, 300, and 1000 ms. The results qualitatively confirm our hypothesis: With the donor in the neutral state during the wait time, the dephasing time remained constant at around $T_2^* \approx 100$ μs, whereas the donor ionization caused T_2^* to drop to 51, 19, and 17 μs for T_{wait} = 100, 300, and 1000 ms, respectively. The above values were obtained on device A; the systematic drop in T_2^* with increasing T_{wait} in the ionized state was further verified on three different single-donor devices (see below in the section 'Parameter-free numerical model of nuclear freezing and unfreezing').

The hypothesis of nuclear freezing by hyperfine interactions can be further cross-checked by replacing the Ramsey experiment with a Hahn echo sequence. The Hahn echo includes a refocusing π pulse between the two $\pi/2$ pulses, which has the effect of canceling

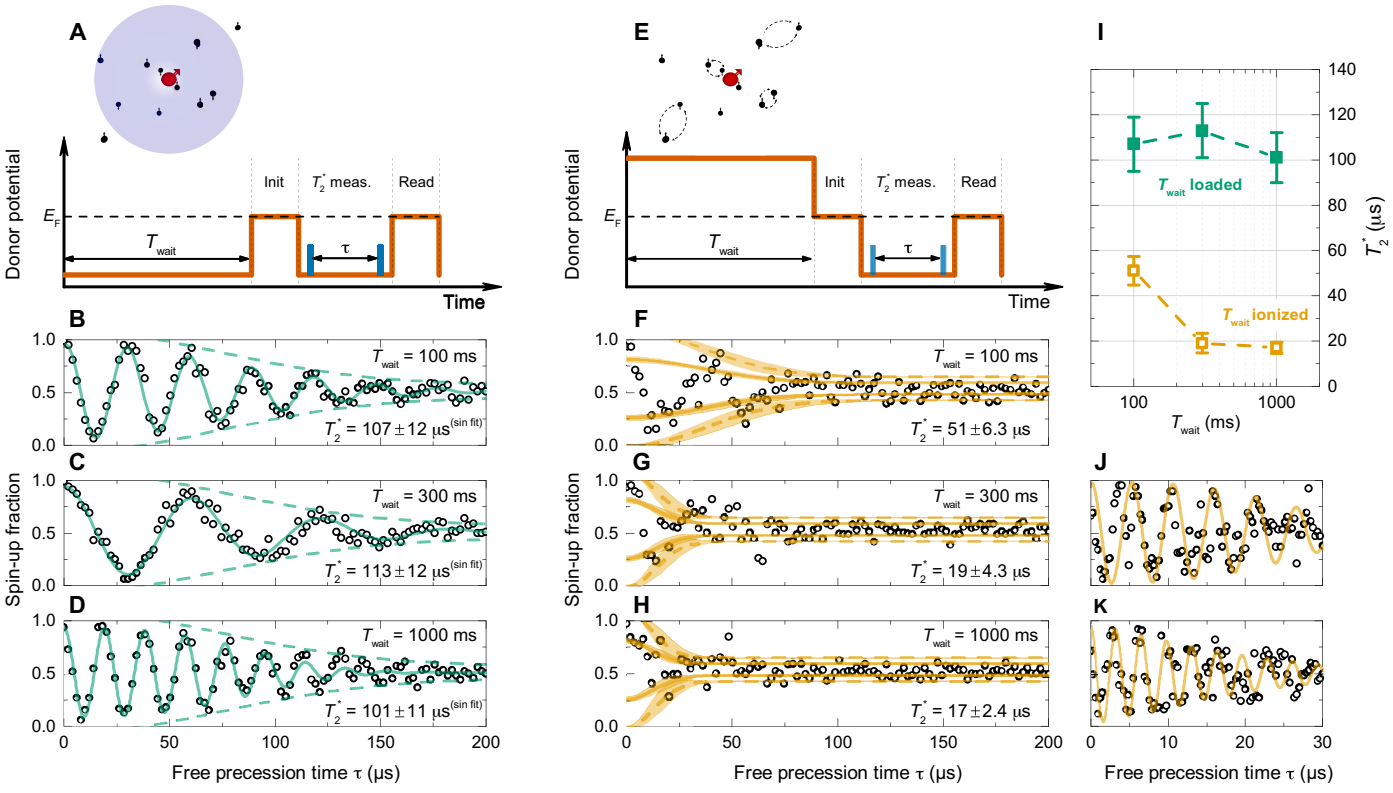

Fig. 2. Experimental freezing and unfreezing of the nuclear spin bath. (**A**) Protocol for a Ramsey experiment to measure the donor electron dephasing time T_2^*, preceding the measurement with a wait time during which an electron is loaded on the donor. (**B** to **D**) Ramsey fringes at increasing wait times T_{wait} = 100, 300, and 1000 ms, as indicated. The solid lines are a fit to Gaussian-decaying sinusoid. The approximately constant T_2^* shows that the nuclear bath is essentially frozen between each run. (**E**) Modified experimental protocol where the wait time is spent with the donor ionized. (**F** to **H**) Ramsey fringes obtained from protocol (E). Here, the wait time with ionized donor allows a dipole-dipole evolution of the nuclear spin bath, resulting in a shortening of T_2^*. Because of the shorter T_2^*, we estimate the envelope decay using a Gaussian SD σ(τ) at each τ and show the single-σ(τ) (solid) and 2σ(τ) (dashed) curves, shaded via the SE confidence interval (see Materials and Methods). (**I**) Values of T_2^* versus T_{wait} with loaded and ionized donor; error bars indicate SE from nonlinear curve fitting. All data are taken on device A. (**J** to **K**) For T_{wait} = 300 and 1000 ms, we cross-check the fitting method by performing the Ramsey experiment with a finer resolution in τ and a larger frequency offset and fitting to a Gaussian-decaying sinusoid.

out the effect of the static randomness of the instantaneous Larmor frequency. This is because the phase accumulated during the first half of the free evolution, $\phi^i_{\tau/2}$, is unwound during the second half by the application of the π-pulse, resulting in a final state that has always $\phi^i_\tau = 0$, unless the phase accumulated between τ/2 and τ is different from the one accumulated between 0 and τ. The decay of the Hahn echo signal thus reveals the presence of random variations of B_{HF} within one run. Therefore, introducing a wait time with the donor in the ionized state before the echo sequence should make no difference for the Hahn echo decay. Figure 3 confirms this expectation: The Hahn echo decay time T_2^{Hahn} remains approximately constant (within the experimental errors) around $T_2^{Hahn} \approx 1.6$ ms, regardless of the length of the ionized-donor wait time introduced before each run.

Parameter-free numerical model of nuclear freezing and unfreezing

We now address whether the reduction of T_2^* agrees quantitatively with reasonable models for nuclear dipole-dipole dynamics. Since the number of ^{29}Si nuclei within the target core of 3.5-nm radius is typically fewer than 10 at 800-ppm concentration, we are able to calculate exactly the evolution of this small spin bath under magnetic dipole-dipole interactions. To do so, we generate baths of randomly located ^{29}Si nuclei at 800-ppm concentration for a simulated set of single phosphorus impurities. We use the bulk values (*19*) for the hyperfine coupling constants A_j and closely mimic the timing of the experiment. The nuclear spin bath evolution is then interrupted by a simulated measurement, which is modeled as the sudden appearance of a spin-down electron spin sometime during the load period (chosen from an exponential distribution with a random tunnel-in lifetime at average 2 ms), and the sudden disappearance of the electron during the ionization period. The ionization can result either from a spin-up measurement (*32*) or from the forcible removal of the electron at the start of the wait period of the next cycle. Millisecond-scale timing details of the pulsing and tunneling have no discernible impact on our simulation results. The important physics in the simulation is the interplay between the hyperfine coupling with the electron and the slow nuclear dipole-dipole interaction, which occurs on much longer time scales. The projected electron spin is logged as a perfect single-shot measurement, and the averaged results are fit to Gaussian decay as a function of τ, just as in the Ramsey experiment. Further details appears in Materials and Methods.

Figure 4 (A to E) shows examples of simulated traces of the time-dependent Overhauser shift, defined as $\delta\omega_e(t) = \sum_j A_j \langle I_j^z(t) \rangle$, which

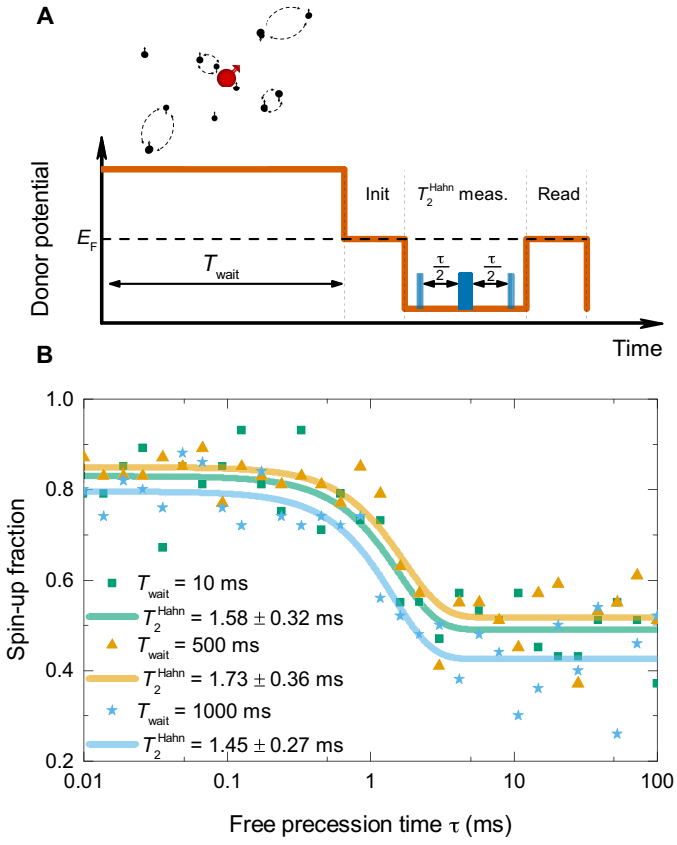

Fig. 3. Cross-check of nuclear freezing hypothesis by a Hahn echo experiment. (**A**) Experimental protocol for a Hahn echo experiment to obtain the electron coherence time T_2^H, preceding the measurement with a wait time T_{wait} with donor ionized. (**B**) All Hahn echo decays show a similar value of T_2^H, as expected from the insensitivity of the Hahn echo measurement to changes in the static Overhauser field from run to run. Data are taken on device B.

acts as a drifting noise on the electron spin qubit. As a result of this drift, simulated Ramsey experiments show varying T_2^* decay time scales, depending on the wait time T_{wait} preceding each run. Example fits to the Ramsey decay for five simulated wait times are shown in Fig. 4 (F to J).

Figure 5A summarizes the values of T_2^* as a function of the wait time with an ionized donor, obtained experimentally in three different devices, alongside the numerical simulations (Fig. 5B) obtained for six different random placements of ^{29}Si nuclei. Similar simulations for many more configurations were also performed, and it was found that these do not significantly contribute to the spread of T_2^* values shown. The qualitative and even quantitative trend of T_2^* as a function of T_{wait} shows good agreement between theory and model, especially for long T_{wait} where the nuclear spin dynamics provide the dominant source of dephasing. This is rather remarkable, considering that the model is essentially parameter free. The only variable in the model, and also in experimental results obtained from different samples, is simply the random placement of the ^{29}Si nuclei.

While our model captures key elements of the frozen-core hypothesis and its experimental test, it omits some factors that can have an impact on the experimental results. Intrinsic factors are the ensemble of nuclear spins outside the inner electron core, while an extrinsic one is, e.g., the magnetic noise arising from the superconducting solenoid that produces the B_0 field (*10*). These omitted factors are likely to be the main contribution to the finite experimental values of T_2^* as $T_{wait} \to 0$, since the model predicts a completely frozen nuclear bath when the electron is present. Other omitted factors include the effects of anisotropic hyperfine interactions, for which preliminary numerical investigations indicate negligible effect at the high magnetic fields used here, but would have increasing importance at much lower magnetic fields, as recently observed in metal-oxide semiconductor quantum dots in the same ^{28}Si material with 800-ppm ^{29}Si (*33*).

Hyperfine noise spectrum

The simulation also provides a glimpse into the plausible low-frequency noise spectrum of nuclear Overhauser field that couples to the electron qubit. Figure 6A shows example noise PSDs of the frequency shift $\delta\omega_e(t)$ caused by Overhauser fields, each calculated for five different values of T_{wait} for one isotopic configuration. With frequent electron interactions (short T_{wait}), the spectrum approaches a $1/\omega^2$ power law; in this case, the noise is dominated by a Brownian random walk due to "ionization shock" (*31*, *34*), i.e., the sudden reconfiguration in effective magnetic field seen by each nuclear spin due to the diabatic appearance or disappearance of the neutralizing electron. The forcible removal of the hyperfine-coupled electron is unique to our experiment; however, similar "sudden shock" effects occur also in conventional pulsed-electron paramagnetic resonance, when a fast rotation of the electron spin causes a sudden reorientation of the hyperfine field on the nearby nuclei (*35*).

More notably, when making infrequent measurements (long T_{wait}), the spectrum has a reduced slope approaching a $1/\omega$ power law, reminiscent of noise in spin glasses (*36*). Note that these spectra, as shown in Fig. 6A, are not samples of one large, measurement-insensitive spectral density. The amplitude and exponent for the noise vary drastically, depending on how often electron interactions interrupt coherent dipole-dipole evolution, indicating that the relative amount of backaction plays a key role in determining the spectral noise properties for this system. This is a critical feature, as it indicates strong deviations from a classical Markovian model: Since we must interact the electron with the nuclear bath to measure it, and that interaction strongly perturbs the nuclear bath, the noise spectrum depends critically on our measurement of it [we note that measurement backaction effects in spin echo, even for the much larger nuclear ensembles of GaAs, have been well studied (*37*)].

The simplicity and small Hilbert space size of the ^{31}P donor system in a bath of ^{29}Si nuclei at 800-ppm concentration have thus allowed us to provide numerically accurate estimates of the hyperfine noise PSD. However, this brute-force approach would quickly become inapplicable to larger systems or denser nuclear baths. We may therefore ask what classical noise models could serve as a suitable approximation to the nuclear dipolar dynamics. For this, we use the language of filter functions, in which the application of control pulses to the electron spin qubit is likened to applying a filter to an independent noise process that couples to the qubit (*38*, *39*). The precise spectral properties of the filter depend on the sequence and timing of the control pulses. The filter function for a Ramsey experiment is mostly sensitive to the "zero-frequency" component of the noise spectral density, which is often modeled under ergodic, "quasistatic" assumptions as some run-to-run variation in a static frequency offset. However, when we abandon assumptions of ergodicity, we must ask how the process of averaging

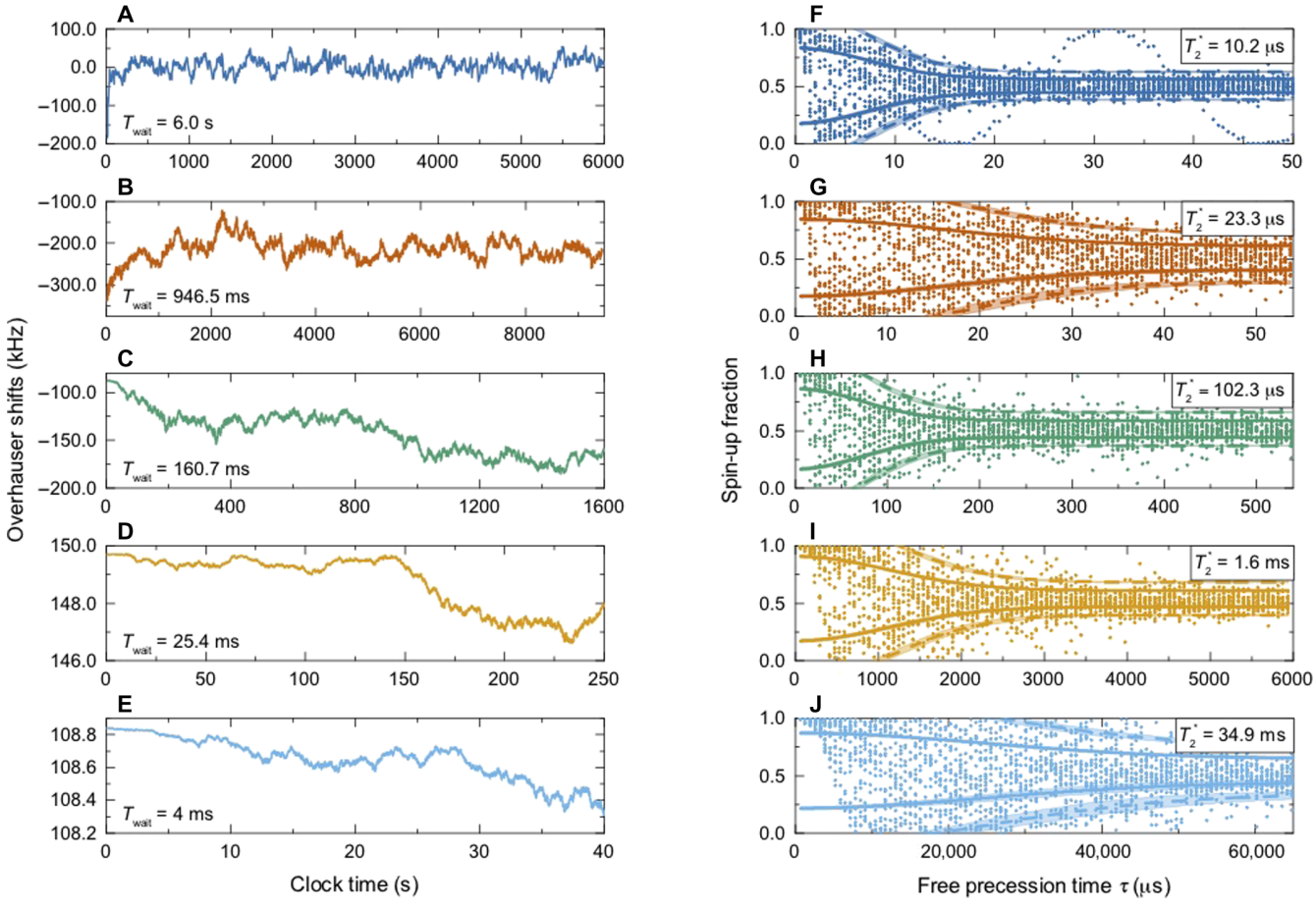

Fig. 4. Parameter-free simulation of Overhauser noise. (**A** to **E**) Numerically simulated Overhauser shifts resulting from ^{29}Si nuclear dipolar dynamics while keeping the donor ionized for five different values of wait time T_{wait}, interrupted by Ramsey measurements on the electron spin. (**F** to **J**) Corresponding time-averaged T_2^* measurements, resulting from 20 independent simulated experiments for a single arrangement of ^{29}Si nuclei, superimposed. Occasionally, a single simulated experiment has much less Overhauser drift than the others, resulting, e.g., in the visibly long-lived sinusoid in (F). All ensemble members, including these outliers, are fit together to estimate T_2^*. T_2^* is seen to reduce drastically as wait time T_{wait} is increased, corresponding to additional nuclear diffusion during the ionized interval. The solid line shows the σ-point, and the dashed line shows the 2σ-point of the fit of the decaying distribution of simulated measurement results, shaded via the SE confidence interval.

over many repetitions (for a total duration of several seconds) affects the sensitivity to very low–frequency noise components. A derivation provided in Materials and Methods yields an approximate filter function for N averages with wait time T between measurements as

$$F(\omega; N, T) \approx \left[1 - \frac{\sin(N\omega T)}{2N \sin(\omega T/2)}\right] \quad (3)$$

In the presence of an input magnetic field noise with spectral density $S_B(\omega)$, the variance of the magnetic field noise observed in an experiment can be estimated as

$$\sigma_B^2 = 2\left(\frac{1}{T_2^*}\right)^2 = \int_0^\infty \frac{d\omega}{2\pi} S_B(\omega) F(\omega; N, T) \quad (4)$$

Following (*18*), the simplest noise model we may use is the Ohrenstein-Uhlenbeck process, which likens nuclear drift to Brownian motion with friction. This provides a Gaussian, Markovian, stationary process characterized by a simple exponential autocorrelation function with correlation time τ_c. Hence, the model for the PSD of the noise, integrating to a total noise power σ_0^2, would, in this case, be

$$S_B(\omega) = \frac{4\sigma_0^2}{\tau_c} \frac{1}{1 + (\omega\tau_C)^2} \quad (5)$$

Inserting this in Eq. 4, the anticipated T_2^* measured as a function of the duration of each run, $T \approx T_{wait}$, becomes

$$\frac{1}{(T_2^*)^2} = 2\sigma_0^2\left[1 - \frac{e^{-T/\tau_c}}{N} \frac{1 - \exp(-NT/\tau_c)}{1 - \exp(-T/\tau_c)}\right] \quad (6)$$

This functional dependence of T_2^* on $T \approx T_{wait}$ may be fit with the experimental data of Fig. 5A. Using $N = 100$ for the number of single runs at each value of τ, fits to that data provide correlation times varying between half a second and half an hour for the three samples. This is consistent with the simulation results in (*18*), which uses cluster-expansion techniques to similarly simulate bath dynamics

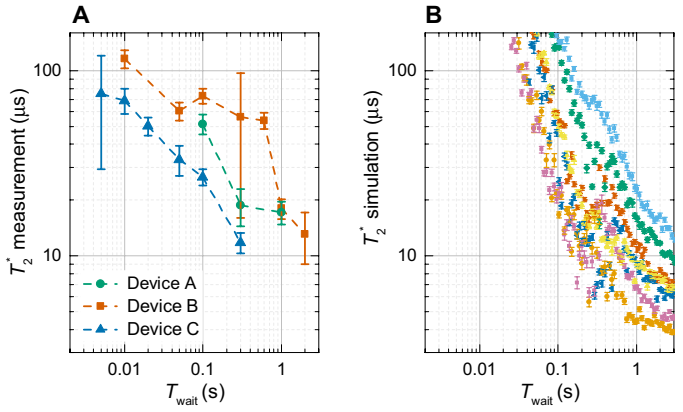

Fig. 5. Electron dephasing time versus nuclear dynamics: Experiment and simulation. (**A**) Experimental electron dephasing time T_2^* as a function of wait time T_{wait} in the ionized state, for three different devices as indicated. (**B**) T_2^* extracted from parameter-free numerical simulations, mimicking the timing of the experiment and using the same fitting procedure. Six randomly chosen nuclear configurations are indicated by color; there is no color correlation to the three experimental devices. In both plots, error bars result from the SE from nonlinear curve fitting.

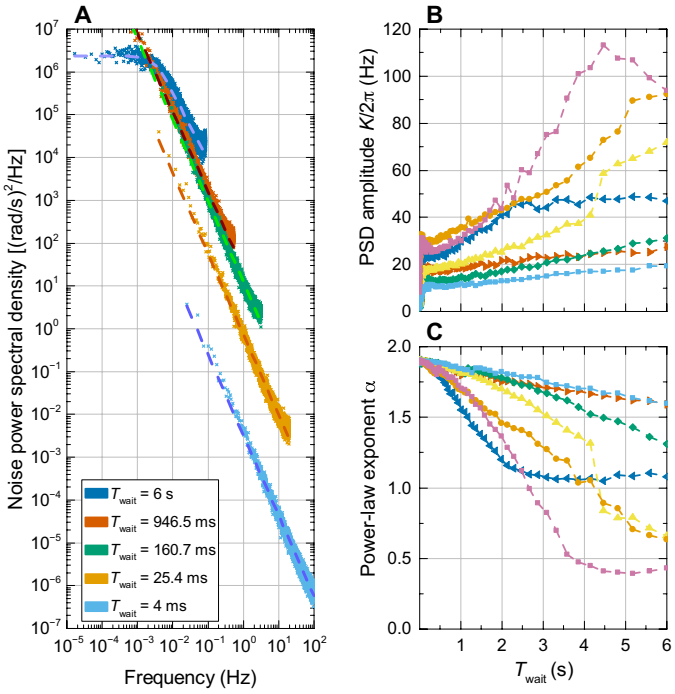

Fig. 6. Simulation of Overhauser noise spectral densities to power law. (**A**) PSD of the Overhauser field fluctuations, obtained from parameter-free numerical simulations such as those shown in Fig. 4 (A to E), for the five different ionized wait times T_{wait}, as indicated. Dashed lines are fits to Eq. 7, where the PSD is parametrized by an amplitude K and a power-law exponent α. (**B**) PSD amplitude $K/2\pi$ and (**C**) power-law exponent α as a function of T_{wait}, obtained from fitting Eq. 7 to numerical simulations for six different isotopic configurations, matching Fig. 5B.

in six different nuclear configurations, fitting the autocorrelation functions to exponentials and finding a broad range of correlation times.

However, many possible models may fit with the experimental data. A key role of the numerical simulation data is to provide a higher density of data without error sources beyond those expected from the noise model in question, and for the data in Fig. 5B, we find that Eq. 6 is a poor fit. This should not be unexpected for two key reasons: First, the noise source is not independent of measurement, as we have indicated, and second, when measurement is infrequent, the Overhauser noise PSDs of Fig. 6A poorly match Eq. 5, appearing instead to follow a more general $1/\omega^{\alpha}$ power law with low-frequency roll-off.

These observations suggest that the Ohrenstein-Uhlenbeck process may not be an adequate description on the nuclear bath dynamics in a system undergoing infrequent measurement. It may be more appropriate to instead characterize the simulated noise using the empirical function

$$S_B(\omega) = \frac{2\pi K^2}{\omega_0}\left[\frac{\omega_0}{\omega_1}\tan^{-1}\left(\frac{\omega_1}{\omega}\right)\right]^{\alpha} \quad (7)$$

and find an effective amplitude K, slope α, and low-frequency roll-off ω_1 by fitting to simulated PSD functions; examples of which are shown in Fig. 6A. The parameter ω_0 is taken as 2π rad/s to maintain units of seconds^{-1} for K. The fit values of K and α for six simulated samples over a range of T_{wait} are shown in Fig. 6 (B and C). We note that the low-frequency roll-off ω_1 occurs in our simulations largely due to the finite number of nuclei considered, leading to a finite lower bound to the dipolar Hamiltonian, and likely does not well inform the case of a real donor in an extended crystal with thousands of weakly coupled ^{29}Si. If we numerically integrate Eq. 7 with Eq. 4, we then find a T_2^* varying with T_{wait} in good correspondence with the simulated measurements, indicating that treating the underlying Overhauser fluctuations as a classical noise bath with general $1/\omega^{\alpha}$ power law provides a useful model, but noting that K and α depend sensitively on how often the nuclei interact with the measuring electron spin.

Of course, the $1/\omega^{\alpha}$ noise from the ^{29}Si nuclear bath cannot persist at frequencies higher than allowed by the dipole-dipole dynamics driving the noise. Already at a kilohertz range, the noise must roll off, and a dynamical decoupling experiment such as Hahn echo should be insensitive to this wait time–dependent drift, as confirmed by the experimental data in Fig. 3. The echo decay at rate T_2^{Hahn} is dominated by residual noise in the kilohertz range. Here, ensemble experiments (*6*) [and supporting theory; (*9*)] show that the intrinsic T_2^{Hahn} for this ^{29}Si concentration is tens of milliseconds. The much shorter $T_2^{Hahn} \approx 1.6$ ms reported here and in other single-donor experiments suggests that other sources of noise (*10*, *40*), not accounted for in the present simulations, must be responsible for the observed Hahn echo decay.

Comparison to other physical systems

Standard models of spin diffusion, lacking nuclear freezing effects, predict an Overhauser field "brown noise" spectrum with α = 2 (*16*–*18*). Conversely, our experiments and simulations unveiled a PSD resembling more a "pink noise" of the form $1/\omega^{\alpha}$, with α < 2. As seen in Fig. 6C, at $T_{wait} \to 0$, the spectrum certainly behaves as an α = 2 power law, but here, it is due to the telegraph noise–like influence of the dephasing from frequent measurement rather than spin diffusion effects. Spin diffusion effects become more important as the nuclear bath is unfrozen, i.e., with increasing T_{wait}, for which the exponent α decreases. The resulting pink noise for mostly empty donors is consistent with the direct observation of $1/\omega$ nuclear noise in isotopically enriched Si/SiGe quantum dots (*41*). There, the dots

are empty or contain two hyperfine-inactive singlet electrons during most of the experiment, allowing free nuclear dipole-dipole interaction for the duration of the experiment, and T_2^* times are close to the ergodic limit. Spectral drift due to nuclear spins in isotopically enriched metal-oxide-semiconductor (MOS) dots also shows $1/\omega^{\alpha}$ spectral characteristics (*21*), suggesting that this is a common behavior in silicon, where the nuclear spins appear in a dilute, disordered lattice, in contrast to widely studied dense nuclear spin crystals such as GaAs or CaF_2. Theoretical validation of $1/\omega$ dipolar dynamics in larger quantum dot systems cannot be achieved with the brute-force numerical methods adopted here and will require more advanced simulation techniques such as coupled cluster expansions (*18*).

Another interesting open question is whether, in general, the whitening of the Overhauser dipolar noise corresponds to a change in the resonance line shape (*16*). It is well known that a dense ensemble of dipolarly coupled spins results in a Gaussian line shape, which turns into a Lorentzian if the spins become sparse upon spatial dilution (*20*). The same effect can be found as a function of temperature, since the spin excitations become more sparse when the thermal energy is lower than the energy splitting of the individual spins (*42*). Here, we have only considered the second moment of the resonance line (the Fourier transform of the Ramsey decay) via the noise spectral density, and we have assumed a Gaussian decay, which is not necessarily the best possible fit to all experimental or numerical data. Since our concern in this study is the lowest-order autocorrelation of the noise, these higher-order line shape effects fall outside the scope of the present study, but we envisage that this line of investigation might in the future shed light on the general relationship between noise spectra and line shapes.

A $1/\omega$ noise spectrum has been observed in multiple recent experiments on isotopically enriched silicon devices, each including deliberate magnetic field gradients generated by locally fabricated micromagnets (*43*, *44*). As these studies verify, in these cases, the $1/\omega$ noise results from device electric-field noise transduced into magnetic-field noise due to the strong gradient. Of course, there are certainly nuclear freezing effects in these experiments due to not only the hyperfine field of the electrons at play but also the micromagnetic gradients. Because of these additional complications, the present results are difficult to apply to these systems, requiring further simulation work incorporating classical, macroscopic field gradients.

DISCUSSION

The experiments and theoretical analysis presented here provide conclusive evidence that the presence of a hyperfine-coupled electron can markedly slow down the dynamics of a bath of nuclear spins. This observation can have important consequences on the operation of a spin-based quantum computer in semiconductors, especially in the context of achieving quantum gate fidelities, surpassing some fault-tolerance threshold.

At finite isotopic purification, high gate fidelities in the presence of fluctuating Overhauser fields will quite certainly demand the use of dynamically corrected gates and/or frequent recalibration of the qubit frequency. Examples already exist, where dynamical recalibration and compensation sequences have substantially extended T_2^* and reduced gate errors in quantum dot systems, both in GaAs (*45*, *46*) and in isotopically purified silicon (*21*, *47*). While these methods are known to be effective at the one- or two-qubit level, the operation of a large-scale spin-based quantum processor is likely to benefit from the ability to achieve high-fidelity gates without the need for frequency recalibration.

In this context, our work provides a simple recommendation: Wherever possible, introduce a hyperfine-coupled electron to freeze out the nuclear bath. This may be especially pertinent in singlet-triplet qubit systems using isotopically enriched Si, where the frequent presence of empty dots or hyperfine-inactive singlets lead to T_2^* at the ergodic limit and introduces associated limits to control fidelity (*48*). The experiments and models presented here suggest that a redesign of the experimental protocols in these systems to maximize the time each dot spends containing an odd number of hyperfine-coupled electrons may improve overall fidelity and reduce the need for frequent recalibration. Hence, we believe that our explorations into the very low–frequency character of nuclear dipole dynamics in single phosphorus impurities may assist the engineering of high-fidelity quantum logic gates in a broad class of semiconductor-based future quantum processors.

More broadly, our observations of controllable freezing of a nuclear spin bath may, in the future, provide an interesting platform in which to study many-body localization and thermalization in disordered systems with random interactions (*49*).

MATERIALS AND METHODS

Experimental methods

Details on the fabrication and operation of our implanted single-donor devices may be found in (*10*). The devices were mounted on the mixing chamber of a dilution refrigerator with a typical electron temperature of 100 mK and subjected to a static magnetic field $B^z \approx$ 1.4 T created by a superconducting solenoid. Coherent electron spin control was achieved by irradiating the spin with oscillating magnetic fields at microwave frequencies (typically around 40 GHz) delivered by an on-chip coplanar waveguide terminated by a short circuit (*50*). The electron spin state at the end of each experimental run was measured in a single shot using the well-established spin-dependent tunneling method. This is achieved by tunnel coupling the donor to a cold charge reservoir and detecting the spin-dependent ionization of the donor with a single-electron transistor (SET). The SET is fabricated in proximity of the ion-implantation region (*32*), where a small number of ^{31}P donors was implanted with energies of 10 (device A) or 14 keV (devices B and C) per ion. In our devices, the cold charge reservoir is the SET island itself.

Ramsey data fitting

Although the Ramsey experiment is a common procedure, the extracted values of T_2^* can depend not only on averaging times and wait times but also on the method chosen for curve fitting. For both the experiment and the theory, finite averaging effects result in notable variation in T_2^*, depending on how the decaying sinusoidal Ramsey fringes are fit. One option for fitting is to attempt a direct nonlinear fit to the decay function $P_{\uparrow}(\tau) = C_0 + C_1 \cos(\Delta\omega \cdot \tau) \exp[-(\tau/T_2^*)^2]$, as used in Fig. 2 (A to C and J to K). However, for large variations of the average detuning $\delta\omega_e(t)$, this fit may easily fail. A more robust option when focusing on T_2^* is to ignore the oscillating component of the Ramsey fringes and fit instead the envelope of the observed decay. We do so, both for experiments and simulations, by taking multiple traces of the Ramsey oscillation curve and finding a least-squares fit between the data at each delay τ and a normal distribution with SD $\sigma(\tau)$, constrained so that $\sigma(\tau)$ follows an offset

Gaussian decay $\sigma(\tau) = \sigma_0 + \sigma_1 \exp[-(\tau/T_2^*)^2]$. In Figs. 2 (E to H) and 4 (F to J), the fit outcomes $\sigma(\tau)$ and $2\sigma(\tau)$ are shown, shaded according to a confidence interval using the $1-\sigma$ SE, resulting from the Levenberg-Marquardt nonlinear least-squares algorithm. This fitting procedure is also insensitive to errors due to imperfect initialization and measurement visibility. Notably, the parameter T_2^* in this and in most other studies tracks the decay of an averaged sinusoid but discards the information of the sinusoid's center frequency. This results in an effective insensitivity to the lowest-frequency drifts in the system and hence, provides, in conjunction with the averaging time over the full experiment, the effective low-frequency cutoff of the noise spectrum to which the experiment is sensitive.

Numerical simulations

The complete Hamiltonian of the simulated model is

$$H = H_{\text{dipolar}} + n(t)\,H_{\text{HF}} - n(t)\,g\mu_B B^z S^z - \sum_k \hbar\gamma B^z I_k^z \tag{8}$$

The latter two terms here are the electron and nuclear Zeeman energies, which we may subsume into a rotating frame. The secular term of the nuclear-nuclear dipolar interaction in this rotating frame (*16*) is then

$$H_{\text{dipolar}} = \frac{\mu_0}{4\pi}(\hbar\gamma)^2 \sum_{j<k} \frac{1-3\cos^2\theta_{jk}}{2\,r_{jk}^3}(\mathbf{I}_j \cdot \mathbf{I}_k - 3\,I_j^z I_k^z) \tag{9}$$

where $\mathbf{I}_k$ is the spin operator for the kth spin-1/2 ^{29}Si nucleus, $\gamma/(2\pi) = -8.5$ MHz/T is the ^{29}Si gyromagnetic ratio, θ_{jk} is the angle between the vector, connecting nuclear spins j and k and the applied magnetic field B^z, and r_{jk} is the distance between those spins. The coupling constants here range from a few millihertz to about a hertz. The secular hyperfine interaction H_{HF} was discussed in Introduction as Eq. 1. The crucial component of the model is to account for the donor charge via the variable $n(t)$. Upon donor ionization, $n(t) = 0$ removes the hyperfine and electron Zeeman terms from the Hamiltonian.

We simulate the experiment in which a Ramsey sequence is performed, but between each single run, the donor electrochemical potential is chosen to ensure that it is ionized [$n(t) = 0$] for a time T_{wait}. During this time, the nuclear spins undergo free evolution according to H_{dipolar}. Then, a $|\downarrow\rangle$ electron is loaded [$n(t) = 1$] to begin the run. Each simulated Ramsey measurement subroutine includes the following components:

(i) The calculation of the Overhauser shift extracts $\delta\omega_e = \sum_k A_k \langle\psi\,|\,I_k^z\,|\,\psi\rangle$ directly from the simulation data.

(ii) The electron spin measurement probability distribution for a Ramsey experiment is calculated as

$$P_{\uparrow,\downarrow} = \frac{1}{2} \pm \frac{1}{2}\cos\{[\Delta\omega_e + \delta\omega_e]\tau\} \tag{10}$$

where $P_\uparrow$ (corresponding to +) and $P_\downarrow$ (corresponding to −) are the spin-up and spin-down probabilities, respectively. The fixed detuning $\Delta\omega_e$ includes a deliberate offset from the Larmor frequency, plus any initial Overhauser shift from the start of the simulation. Using sufficient $\Delta\omega_e$ to see fringe contrast assists curve fitting, but we find that the precise value of it has no discernible impact on our results.

(iii) The simulated single-shot readout result is randomly chosen by drawing a binomial random variable according to $P_{\uparrow,\downarrow}$; we notate the random result as m, which takes values +1/2 for spin up and −1/2 for spin down.

(iv) To determine a dephasing operator corresponding to initialization and measurement, we note that the principal source of backaction randomness is not the measurement itself but rather the uncertain duration of time the electron occupies the donor between tunnel events to and from the reservoir. The essence of the randomness is to assume that during the interval in which an electron is initialized, $t_{\text{init}} = 100$ ms, the actual time it takes for the electron to tunnel in is exponentially distributed with time scale t_{tunnel}, which we estimate as 2 ms, and similarly, for measurement. The corresponding t_{tunnel}^2 variance results in a corresponding hyperfine phase variance $(A_j t_{\text{tunnel}})^2$ on nucleus j. Hence, the simulated measurement and reinitialization process proceeds as follows: The simulation draws a random tunnel-in time t_1 for an electron to occupy the donor from the cumulative distribution function (CDF) $1 - \exp(-t_1/t_{\text{tunnel}})$. The duration of the two ESR $\pi/2$ pulses and the Ramsey free evolution is treated as negligible for the nuclear dynamics. Once loaded, the electron remains on the donor for a time t_2, which may be one of two choices, depending on m. If $m = 1/2$, then t_2 is a tunneling time drawn from the CDF $1 - \exp(-t_2/t_{\text{tunnel}})$.

If $m = -1/2$, then t_2 is the sum of the 100-ms read time and a random tunnel-out time, similarly sampled. The backaction on the nuclear spins for this process is then captured by applying the dephasing operator

$$U_{\text{dephase}} = \exp\big[-i(t_{\text{load}} - t_1)\langle -1/2\,|\,_e H_{\text{HF}}\,|\,-1/2\rangle_e - \text{it}_2(m)\langle m\,|\,_e H_{\text{HF}}\,|\,m\rangle_e\big] \tag{11}$$

where t_1, t_2, and m are random numbers from shot to shot, hence causing phase scrambling within the nuclear ensemble. We have verified that our results do not depend critically on the m dependence of the model; these spin-projection details are in place to mimic the experiment, but a simpler model that only captures a random electron interaction time could be used to obtain similar results, possibly allowing simpler analytic approximations.

This simulated measurement subroutine is repeated N_{meas} times. It is embedded into the full nuclear simulation as follows:

1) Randomly populate a sphere of unstrained silicon lattice sites about 3.5 nm around a donor with random ^{29}Si nuclei at 800-ppm density.

2) Choose a random nuclear spin state $|\psi\rangle$ via coin flipping.

3) Choose a T_{wait} value and calculate

$$U_{\text{evolve}} = \exp(-iH_{\text{dipolar}}\,T_{\text{wait}}) \tag{12}$$

4) For $N_\tau \times N_{\text{meas}}$ cycles, incrementing the value of τ every N_{meas} cycles,

(i) Apply U_{evolve} to $|\psi\rangle$.

(ii) Simulate the Ramsey experiment, as described above.

(iii) Record the average of those N_{meas} single-shot measurements.

5) Curve fit the averaged measurements at each τ to a Gaussian decay to extract T_2^*.

This whole process is then repeated N_{ens} different times and for an array of different wait times T_{wait}. The independent N_{ens} ensemble members use the same configuration of nuclei, but with different initial nuclear spin states (and independent statistics for simulating single-shot measurements). We note that N_{meas} and N_τ dictate the amount of time averaging affecting the observed T_2^* and so are chosen to mimic the experiment in the simulations presented here. In

contrast, N_{ens} ensemble members "reset" the clock and fully scramble nuclei. Parallelized simulations use $N_{ens} = 20$, while serialized experiments use $N_{ens} = 2$.

Filter function across many averages

In this section, we consider the general problem of measuring the frequency of a signal when that frequency drifts substantially over a time scale much slower than the duration of a single measurement but faster than the overall time it takes to make an ensemble of measurements. We approach the problem using a filter-function formalism. While this formalism is well known, a formal treatment of handling noise correlations from measurement to measurement, as opposed to noise correlations during a single pulse sequence, is rarely considered.

Consider a zero-mean angular frequency shift x (e.g., an Overhauser shift), which we seek to measure via a Ramsey-like measurement, meaning that an ensemble of measurements in which a probe (e.g., an electron spin) precesses at drifting frequency $\omega_0 + x(t)$ for a varying time τ, generating a single-shot measurement probability

$$R(t;\tau) = A + B\cos\left(\omega_0\tau + \int_t^{t+\tau} dt' x(t')\right) \tag{13}$$

Here, A and B are irrelevant linear scale parameters, capturing measurement details not presently of interest. If our random frequency shift $x(t)$ was stationary and ergodic, then after "sufficient" averaging, we would ignore the absolute time t and assume that after averaging some $N \gg 1$ measurements at different times t_n

$$\frac{1}{N}\sum_{n=1}^{N} R(t_n;\tau) \approx A + B\cos\left[(\omega_0 + \bar{x})\tau\right] \times \exp\left[-\frac{\tau^2}{2}\int_0^\infty \frac{d\omega}{2\pi}\mathrm{sinc}^2\left(\frac{\omega\tau}{2}\right) S_x(\omega)\right] \tag{14}$$

where $S_x(\omega)$ is the noise spectral density of $x(t)$, and the sampled mean value of $x(t)$ is

$$\bar{x} = \frac{1}{N}\sum_{n=1}^{N} x(t_n) \tag{15}$$

The integral in the decay in 14 exhibits the standard filter function, $\mathrm{sinc}^2(\omega\tau/2)$, for a Ramsey-type frequency measurement. This filter is sharply peaked at $\omega = 0$, suggesting that this measurement is sensitive to the "noise at DC," which is poorly defined, and can place excessive reliance on a poorly known or possibly nonexistent low-frequency roll-off of $S_x(\omega)$.

In a slow-drift scenario, x_n cannot be considered ergodic. To make a more appropriate filter in this case, we focus on the notion that each individual measurement queries $x(t)$ at some absolute time t_n for sampling instance n; abbreviate $x(t_n) = x_n$. We essentially assume that x_n is constant but random for the duration of a Ramsey experiment, similar to the quasistatic limit, but we further allow that x_n is not fully randomized from run to run. Instead, it undergoes drifts according to a random stationary process defined by the very low–frequency part of $S_x(\omega)$. The key insight is that the extraction of the mean, $\bar{x}$ according to 15, provides the low-frequency cutoff to the filter function. Our averaging process measures, under an assumption of Gaussian noise

$$\left\langle \frac{1}{N}\sum_{n=1}^{N}\cos\left[(\omega_0 + x_n)\tau\right]\right\rangle = \cos\left[(\omega + \bar{x})\tau\right] e^{-\langle y_n^2\rangle\tau^2/2} \tag{16}$$

where

$$y_n = x_n - \bar{x} \tag{17}$$

Our critical assumption is that although x_n is not ergodic, the deviation y_n from the randomly sampled mean $\bar{x}$ may be considered as such. This means that the ensemble-averaged variance of y_n should be equal to its time-averaged variance over each of the n measurements, i.e.

$$\langle y_n^2\rangle = \frac{1}{N}\sum_n \langle y_n^2\rangle = \frac{1}{N^2}\sum_{nm}\left[\langle x_n^2\rangle - \langle x_n x_m\rangle\right] \tag{18}$$

The result of this assumption is that the low-frequency components of the fluctuations of $x(t)$, which prevent ergodicity in a finite time–averaged experiment, are "absorbed" into the random mean $\bar{x}$. The information of $\bar{x}$ is, in principle, observable as a mean shift relative to ω_0, but since the true value of ω_0 may be unknown (or irrelevant), the information of the sampled $\bar{x}$ is lost (or ignored), and the experimentally extracted T_2^* may be taken as $\sqrt{2/\langle y_n^2\rangle}$.

We may now cast this simple characterization as a filter function by introducing again the noise spectral density of $x(t)$ via the Wiener-Khinchin theorem and the assumption that the time between sampling x_n and x_m is $T \times (m - n)$ for single-measurement time T, giving the variance

$$\langle y_n^2\rangle = \frac{1}{N}\sum_{m=0}^{N-1}\int_0^\infty \frac{d\omega}{2\pi} S_x(\omega)\left[1 - \cos(\omega m T)\right] = \int_0^\infty \frac{d\omega}{2\pi} F(\omega;N,T)\, S_x(\omega) \tag{19}$$

where

$$F(\omega;N,T) = \frac{(2N-1)\sin(\omega T/2) - \sin\left[(2N-1)\omega T/2\right]}{2N\sin(\omega T/2)} \tag{20}$$

We have, hence, derived a "filter function" $F(\omega; N, T)$ for the long-time diffusion in this experiment. Usually, we choose $N \gg 1$, in which case it simplifies to Eq. 3 of the main text. This equation effectively describes a high-pass filter, with the stop band at frequencies below $1/NT$. This may be added to a decay function using the standard τ-dependent Ramsey filter function $\mathrm{sinc}^2(\omega\tau/2)$ but with an appropriately chosen low-frequency cutoff for the noise.

REFERENCES AND NOTES

1. R. Hanson, L. P. Kouwenhoven, J. R. Petta, S. Tarucha, L. M. K. Vandersypen, Spins in few-electron quantum dots. *Rev. Mod. Phys.* **79**, 1217–1265 (2007).
2. F. A. Zwanenburg, A. S. Dzurak, A. Morello, M. Y. Simmons, L. C. L. Hollenberg, G. Klimeck, S. Rogge, S. N. Coppersmith, M. A. Eriksson, Silicon quantum electronics. *Rev. Mod. Phys.* **85**, 961–1019 (2013).
3. K. M. Itoh, H. Watanabe, Isotope engineering of silicon and diamond for quantum computing and sensing applications. *MRS Commun.* **4**, 143–157 (2014).
4. D. Sabbagh, N. Thomas, J. Torres, R. Pillarisetty, P. Amin, H. C. George, K. Singh, A. Budrevich, M. Robinson, D. Merrill, L. Ross, J. Roberts, L. Lampert, L. Massa, S. V. Amitonov, J. M. Boter, G. Droulers, H. G. J. Eenink, M. van Hezel, D. Donelson, M. Veldhorst, L. M. K. Vandersypen, J. S. Clarke, G. Scappucci, Quantum transport properties of industrial $^{28}Si/^{28}SiO_2$. *Phys. Rev. Appl.* **12**, 014013 (2019).
5. J. P. Gordon, K. D. Bowers, Microwave spin echoes from donor electrons in silicon. *Phys. Rev. Lett.* **1**, 368–370 (1958).
6. A. M. Tyryshkin, S. A. Lyon, A. V. Astashkin, A. M. Raitsimring, Electron spin relaxation times of phosphorus donors in silicon. *Phys. Rev. B* **68**, 193207 (2003).

7. A. M. Tyryshkin, S. Tojo, J. J. L. Morton, H. Riemann, N. V. Abrosimov, P. Becker, H.-J. Pohl, T. Schenkel, M. L. W. Thewalt, K. M. Itoh, S. A. Lyon, Electron spin coherence exceeding seconds in high-purity silicon. *Nat. Mater.* **11**, 143–147 (2012).
8. W. M. Witzel, X. Hu, S. Das Sarma, Decoherence induced by anisotropic hyperfine interaction in Si spin qubits. *Phys. Rev. B* **76**, 035212 (2007).
9. W. M. Witzel, M. S. Carroll, A. Morello, L. Cywiński, S. Das Sarma, Electron spin decoherence in isotope-enriched silicon. *Phys. Rev. Lett.* **105**, 187602 (2010).
10. J. T. Muhonen, J. P. Dehollain, A. Laucht, F. E. Hudson, R. Kalra, T. Sekiguchi, K. M. Itoh, D. N. Jamieson, J. C. McCallum, A. S. Dzurak, A. Morello, Storing quantum information for 30 seconds in a nanoelectronic device. *Nat. Nanotechnol.* **9**, 986–991 (2014).
11. J. T. Muhonen, A. Laucht, S. Simmons, J. P. Dehollain, R. Kalra, F. E. Hudson, S. Freer, K. M. Itoh, D. N. Jamieson, J. C. McCallum, A. S. Dzurak, A. Morello, Quantifying the quantum gate fidelity of single-atom spin qubits in silicon by randomized benchmarking. *J. Phys. Condens. Matter* **27**, 154205 (2015).
12. J. P. Dehollain, J. T. Muhonen, R. Blume-Kohout, K. M. Rudinger, J. K. Gamble, E. Nielsen, A. Laucht, S. Simmons, R. Kalra, A. S. Dzurak, A. Morello, Optimization of a solid-state electron spin qubit using gate set tomography. *New J. Phys.* **18**, 103018 (2016).
13. J. J. Pla, K. Y. Tan, J. P. Dehollain, W. H. Lim, J. J. L. Morton, D. N. Jamieson, A. S. Dzurak, A. Morello, A single-atom electron spin qubit in silicon. *Nature* **489**, 541–545 (2012).
14. J. H. Van Vleck, The dipolar broadening of magnetic resonance lines in crystals. *Phys. Rev.* **74**, 1168–1183 (1948).
15. W. A. Coish, D. Loss, Hyperfine interaction in a quantum dot: Non-Markovian electron spin dynamics. *Phys. Rev. B* **70**, 195340 (2004).
16. A. Abragam, *The Principles of Nuclear Magnetism* (Clarendon Press, 1961).
17. D. J. Reilly, J. M. Taylor, E. A. Laird, J. R. Petta, C. M. Marcus, M. P. Hanson, A. C. Gossard, Measurement of temporal correlations of the Overhauser field in a double quantum dot. *Phys. Rev. Lett.* **101**, 236803 (2008).
18. W. M. Witzel, K. Young, S. Das Sarma, Converting a real quantum spin bath to an effective classical noise acting on a central spin. *Phys. Rev. B* **90**, 115431 (2014).
19. J. L. Ivey, R. L. Mieher, Ground-state wave function for shallow-donor electrons in silicon. I. Isotropic electron-nuclear-double-resonance hyperfine interactions. *Phys. Rev. B* **11**, 822–848 (1975).
20. E. Abe, A. M. Tyryshkin, S. Tojo, J. J. L. Morton, W. M. Witzel, A. Fujimoto, J. W. Ager, E. E. Haller, J. Isoya, S. A. Lyon, M. L. W. Thewalt, K. M. Itoh, Electron spin coherence of phosphorus donors in silicon: Effect of environmental nuclei. *Phys. Rev. B* **82**, 121201(R) (2010).
21. W. Huang, C. H. Yang, K. W. Chan, T. Tanttu, B. Hensen, R. C. C. Leon, M. A. Fogarty, J. C. C. Hwang, F. E. Hudson, K. M. Itoh, A. Morello, A. Laucht, A. S. Dzurak, Fidelity benchmarks for two-qubit gates in silicon. *Nature* **569**, 532–536 (2019).
22. G. R. Khutsishvili, Spin diffusion and magnetic relaxation of nuclei. *Soviet Phys. JETP* **15**, 909–913 (1962).
23. R. Guichard, S. J. Balian, G. Wolfowicz, P. A. Mortemousque, T. S. Monteiro, Decoherence of nuclear spins in the frozen core of an electron spin. *Phys. Rev. B* **91**, 214303 (2015).
24. J. P. Wolfe, Direct observation of a nuclear spin diffusion barrier. *Phys. Rev. Lett.* **31**, 907–910 (1973).
25. C. E. Bradley, J. Randall, M. H. Abobeih, R. C. Berrevoets, M. J. Degen, M. A. Bakker, M. Markham, D. J. Twitchen, T. H. Taminiau, A ten-qubit solid-state spin register with quantum memory up to one minute. *Phys. Rev. X* **9**, 031045 (2019).
26. M. J. Graham, C.-J. Yu, M. D. Krzyaniak, M. R. Wasielewski, D. E. Freedman, Synthetic approach to determine the effect of nuclear spin distance on electronic spin decoherence. *J. Am. Chem. Soc.* **139**, 3196–3201 (2017).
27. C. Ramanathan, Dynamic nuclear polarization and spin diffusion in nonconducting solids. *Appl. Magn. Reson.* **34**, 409–421 (2008).
28. K. O. Tan, M. Mardini, C. Yang, J. H. Ardenkjær-Larsen, R. G. Griffin, Three-spin solid effect and the spin diffusion barrier in amorphous solids. *Sci. Adv.* **5**, eaax2743 (2019).
29. E. A. Chekhovich, M. Hopkinson, M. S. Skolnick, A. I. Tartakovskii, Suppression of nuclear spin bath fluctuations in self-assembled quantum dots induced by inhomogeneous strain. *Nat. Commun.* **6**, 6348 (2015).
30. T. Botzem, R. P. G. McNeil, J.-M. Mol, D. Schuh, D. Bougeard, H. Bluhm, Quadrupolar and anisotropy effects on dephasing in two-electron spin qubits in GaAs. *Nat. Commun.* **7**, 11170 (2016).
31. J. J. Pla, K. Y. Tan, J. P. Dehollain, W. H. Lim, J. J. L. Morton, F. A. Zwanenburg, D. N. Jamieson, A. S. Dzurak, A. Morello, High-fidelity readout and control of a nuclear spin qubit in silicon. *Nature* **496**, 334–338 (2013).
32. A. Morello, J. J. Pla, F. A. Zwanenburg, K. W. Chan, K. Y. Tan, H. Huebl, M. Möttönen, C. D. Nugroho, C. Yang, J. A. van Donkelaar, A. D. C. Alves, D. N. Jamieson, C. C. Escott, L. C. L. Hollenberg, R. G. Clark, A. S. Dzurak, Single-shot readout of an electron spin in silicon. *Nature* **467**, 687–691 (2010).
33. Z. Zhao, C. Chen, W. Wu, F. Wang, L. Du, X. Zhang, Y. Xiong, X. He, Y. Cai, R. T. K. Kwok, J. W. Y. Lam, X. Gao, P. Sun, D. L. Phillips, D. Ding, B. Z. Tang, Highly efficient photothermal nanoagent achieved by harvesting energy via excited-state intramolecular motion within nanoparticles. *Nat. Commun.* **10**, 768 (2019).
34. S. J. Hile, L. Fricke, M. G. House, E. Peretz, C. Y. Chen, Y. Wang, M. Broome, S. K. Gorman, J. G. Keizer, R. Rahman, M. Y. Simmons, Addressable electron spin resonance using donors and donor molecules in silicon. *Sci. Adv.* **4**, eaaq1459 (2018).
35. A. Schweiger, G. Jeschke, *Principles of Pulse Electron Paramagnetic Resonance* (Oxford Univ. Press, 2001).
36. M. B. Weissman, What is a spin glass? A glimpse via mesoscopic noise. *Rev. Mod. Phys.* **65**, 829–839 (1993).
37. P. Bethke, R. P. G. McNeil, J. Ritzmann, T. Botzem, A. Ludwig, A. D. Wieck, H. Bluhm, Coherent hyperfine back-action from single electrons on a mesoscopic nuclear spin bath. arXiv:1906.11264 [cond-mat, physics:quant-ph] (2019).
38. Ł. Cywiński, R. M. Lutchyn, C. P. Nave, S. Das Sarma, How to enhance dephasing time in superconducting qubits. *Phys. Rev. B* **77**, 174509 (2008).
39. M. J. Biercuk, A. C. Doherty, H. Uys, Dynamical decoupling sequence construction as a filter-design problem. *J. Phys. B Atom. Mol. Opt. Phys.* **44**, 154002 (2011).
40. R. Kalra, A. Laucht, J. P. Dehollain, D. Bar, S. Freer, S. Simmons, J. T. Muhonen, A. Morello, Vibration-induced electrical noise in a cryogen-free dilution refrigerator: Characterization, mitigation, and impact on qubit coherence. *Rev. Sci. Instrum.* **87**, 073905 (2016).
41. K. Eng, T. D. Ladd, A. Smith, M. G. Borselli, A. A. Kiselev, B. H. Fong, K. S. Holabird, T. M. Hazard, B. Huang, P. W. Deelman, I. Milosavljevic, A. E. Schmitz, R. S. Ross, M. F. Gyure, A. T. Hunter, Isotopically enhanced triple-quantum-dot qubit. *Sci. Adv.* **1**, e1500214 (2015).
42. A. Morello, P. C. E. Stamp, I. S. Tupitsyn, Pairwise decoherence in coupled spin qubit networks. *Phys. Rev. Lett.* **97**, 207206 (2006).
43. J. Yoneda, K. Takeda, T. Otsuka, T. Nakajima, M. R. Delbecq, G. Allison, T. Honda, T. Kodera, S. Oda, Y. Hoshi, N. Usami, K. M. Itoh, S. Tarucha, A quantum-dot spin qubit with coherence limited by charge noise and fidelity higher than 99.9%. *Nat. Nanotechnol.* **13**, 102–106 (2018).
44. T. Struck, A. Hollmann, F. Schauer, O. Fedorets, A. Schmidbauer, K. Sawano, H. Riemann, N. V. Abrosimov, Ł. Cywiński, D. Bougeard, L. R. Schreiber, Low-frequency spin qubit energy splitting noise in highly purified ^{28}Si/SiGe. *NPJ Quantum Inf.* **6**, 40 (2020).
45. M. D. Shulman, S. P. Harvey, J. M. Nichol, S. D. Bartlett, A. C. Doherty, V. Umansky, A. Yacoby, Suppressing qubit dephasing using real-time Hamiltonian estimation. *Nat. Commun.* **5**, 5156 (2014).
46. P. Cerfontaine, T. Botzem, J. Ritzmann, S. S. Humpohl, A. Ludwig, D. Schuh, D. Bougeard, A. D. Wieck, H. Bluhm, Closed-loop control of a GaAs-based singlet-triplet spin qubit with 99.5% gate fidelity and low leakage. arXiv:1906.06169 [cond-mat, physics:quant-ph] (2019).
47. C. H. Yang, K. W. Chan, R. Harper, W. Huang, T. Evans, J. C. C. Hwang, B. Hensen, A. Laucht, T. Tanttu, F. E. Hudson, S. T. Flammia, K. M. Itoh, A. Morello, S. D. Bartlett, A. S. Dzurak, Silicon qubit fidelities approaching incoherent noise limits via pulse engineering. *Nat. Electron.* **2**, 151–158 (2019).
48. R. W. Andrews, C. Jones, M. D. Reed, A. M. Jones, S. D. Ha, M. P. Jura, J. Kerckhoff, M. Levendorf, S. Meenehan, S. T. Merkel, A. Smith, B. Sun, A. J. Weinstein, M. T. Rakher, T. D. Ladd, M. G. Borselli, Quantifying error and leakage in an encoded Si/SiGe triple-dot qubit. *Nat. Nanotechnol.* **14**, 747–750 (2019).
49. R. Nandkishore, D. A. Huse, Many-body localization and thermalization in quantum statistical mechanics. *Annu. Rev. Condens. Matter Phys.* **6**, 15–38 (2015).
50. J. P. Dehollain, J. J. Pla, E. Siew, K. Y. Tan, A. S. Dzurak, A. Morello, Nanoscale broadband transmission lines for spin qubit control. *Nanotechnology* **24**, 015202 (2013).

Acknowledgments: We acknowledge helpful conversations with M. Grace and W. Witzel. **Funding:** The research was funded by the Australian Research Council Centre of Excellence for Quantum Computation and Communication Technology (grant no. CE170100012) and the U.S. Army Research Office (contract nos. W911NF-17-1-0200 and W911NF-17-1-0198). We acknowledge support from the Australian National Fabrication Facility (ANFF) and the AFAiiR node of the NCRIS Heavy Ion Capability for access to ion-implantation facilities. K.M.I. acknowledges support from a Grant-in-Aid for Scientific Research by MEXT. T.D.L. acknowledges support from the Gordon Godfrey Bequest Sabbatical grant. The views and conclusions contained in this document are those of the authors and should not be interpreted as representing the official policies, either expressed or implied, of the ARO or the U.S. Government. **Author contributions:** M.T.M. and F.E.H. fabricated the devices, with A.M.'s and A.S.D.'s supervision. A.M.J., B.C.J., D.N.J., and J.C.M. designed and performed the ion implantation. K.M.I. supplied the isotopically enriched ^{28}Si wafer. A.M. and A.L. designed the nuclear freezing experiment. M.T.M. and A.L. performed the measurements and analyzed the data. T.D.L. designed and performed the theoretical modeling. M.T.M., T.D.L., and A.M. wrote the manuscript, with input from all coauthors. **Competing interests:** All authors declare that they have no competing interests. **Data and materials availability:** All data needed to evaluate the conclusions in the paper are present in the paper. Additional data related to this paper may be requested from the authors.

Submitted 25 November 2019
Accepted 22 May 2020
Published 3 July 2020
10.1126/sciadv.aba3442

Citation: M. T. Mądzik, T. D. Ladd, F. E. Hudson, K. M. Itoh, A. M. Jakob, B. C. Johnson, J. C. McCallum, D. N. Jamieson, A. S. Dzurak, A. Laucht, A. Morello, Controllable freezing of the nuclear spin bath in a single-atom spin qubit. *Sci. Adv.* **6**, eaba3442 (2020).